ELSEVIER

Journal of University of Science and Technology Beijing
Volume 15, Number 3, June 2008, Page 261

Materials

Numerical study on fatigue damage properties of cavitation erosion for rigid metal materials

Guogang Wang[1,2], *Guang Ma*[1], *Dongbai Sun*[1], *Hongying Yu*[1], *and Huimin Meng*[1]

1) School of Materials Science and Engineering, University of Science and Technology Beijing, Beijing 100083, China

2) Power Station Technology Division, China Electric Power Research Institute, Beijing 100070, China

(Received 2007-06-26)

Abstract: Cavitation erosion is an especially destructive and complex phenomenon. To understand its basic mechanism, the fatigue process of materials during cavitation erosion was investigated by numerical simulation technology. The loading spectrum used was generated by a spark-discharged electrode. Initiation crack life and true stress amplitude was used to explain the cavitation failure period and damage mechanism. The computational results indicated that the components of different materials exhibited various fatigue lives under the same external conditions. When the groove depth was extended, the initiation crack life decreased rapidly, while the true stress amplitude was increased simultaneously. This gave an important explanation to the accelerating material loss rate during cavitation erosion. However, when the groove depth was fixed and the length varied, the fatigue life became complex, more fluctuant than that happened in depth. The results also indicate that the fatigue effect of cavitation plays an important role in contributing to the formation and propagation of characteristic pits.

Key words: cavitation erosion; microjet; numerical simulation; fatigue analysis; crack initiation; loading spectrum

[*This study was financially supported by the National High-Tech Research and Development Program of China (No.2002AA331080) and the Beijing Important Science Technology Projects (No.H024200050021).*]

1. Introduction

Cavitation bubble collapse is a violent process that generates highly localized, large-amplitude shock waves and microjets in the fluid at the point of collapse. When this collapse occurs close to a solid surface, these intense disturbances generate highly localized and transient surface stresses. Often cavitation damage may be responsible for the initiation of severe structural damage to ship propeller blades, turbo machinery, and hydraulic equipment [1].

Though cavitation erosion is a random event, it has some deterministic characteristics in space and time. There are many experimental rules designed to help engineers evaluate the potential cavitation damage rate in certain applications. However, there remain a number of basic questions regarding the fundamental mechanisms which are unsolved yet.

Most publications on cavitation were focused on cavitation bubble dynamics and the preparation of materials with high resistance to cavitation erosion [2-3]. Many researchers [4] tried to correlate the mechanical properties, such as yield stress (YS), ultimate tensile strength (UTS), hardness, fatigue strength, and strain energy, with erosion resistance of materials. So far, no simple relations between them have yet been found. However, it is generally believed [2] that the cavitation resistance was high with low stacking fault energy.

During cavitation experiments, many characters of fatigue damage were observed in the severe cavitation zones due to the phase transformation and new phase precipitation analysis occurred on the cavitation, Wang *et al.* deduced cavitation damage of the material occurred by combined thermal-mechanical fatigue failure [5], moreover, Wang *et al.* proved that the cavitation erosion of the Fe-Mn-Si-Cr shape memory alloys is a failure of low cycle fatigue and fracture

Corresponding author: Dongbai Sun, **E-mail:** dbsun@mater.ustb.edu.cn

Also available online at www.sciencedirect.com

which propagates along the grain boundaries [6]. Based on the results of previous research, Richman and McNaughton [7] found good correlations between material removal rates and cyclic deformation parameters, which is a strong indication that damage in cavitation erosion is a fatigue process.

To date, few people carried out further study on the cavitation fatigue process and its mechanism. In this article, the numerical simulation technology is applied to study the fatigue failure process of cavitation erosion. In particular, the simplified models of cavitation damage are built where two types of grooves or cracks are hypothesized on the surface. The proposed materials used in the numerical simulation are steels 304SS and BS4360-50D. The variation in initiation crack life and the distributing graph of cycle life have been given and discussed too.

2. Cavitation bubble dynamics and impact model

2.1. Bubble collapse dynamics

The mechanism of cavitation has been studied for decades through bubble dynamics. Rayleigh [8] obtained a theoretical expression for pressure development at a relatively moderate distance outside the spherical boundary of a collapsing bubble. According to this theory, the fluid pressure could become extremely high when bubble collapse was nearly ended, a process known as "implosion". In later the theoretical and experimental studies are emphasizing on realistic jet mechanism [9-10]. A bubble collapsing near a solid boundary can acquire a translational motion toward the boundary. As it moves closer to the boundary, the originally spherical bubble shrinks and its surface becomes folded inwards to form a pole directing at the solid boundary. The damage manifests as pits on the surfaces of the components. Under cyclic loading, microcracks may initiate and emanate from the boundary of each cavitation pit [11].

A micro liquid jet is then formed, which delivers a highly concentrated pressure against the boundary, as shown in Fig. 1, in which R_m is the maximum radius of the bubble, and h is the distance between the bubble centroid and the solid boundary [12]. According to the Kelvin impulse theory, both the migration of the centroid and the direction of the liquid jet are directed toward the boundary [13].

The dynamic characteristics of bubble collapsing near a solid boundary have been investigated by means of numerical simulation and experiments. The simulation results have shown that the most destructive bubbles are those that collapse in close proximity to a solid boundary. Blake *et al.* [11] gave, for the case $h=R_m$, the following expression for the maximum jet speed V_m at the end of the bubble-collapsing phase.

$$V_m = 8.6\sqrt{\frac{\Delta p}{\rho_l}} \tag{1}$$

where $\Delta p = p_a - p_v$ is the difference between ambient pressure p_a and liquid vapor pressure p_v, and p_a is the density of the liquid. Eq. (1) was found to be in good agreement with the experimental results.

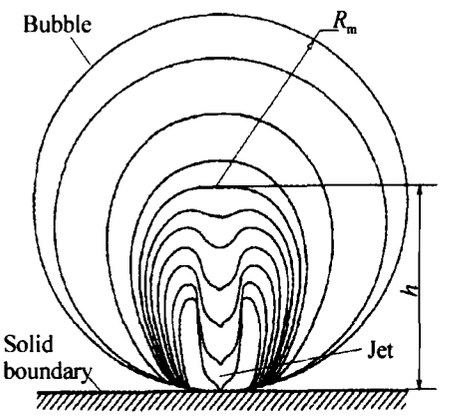

Fig. 1. Bubble collapsing process near a solid boundary [14].

The impact pressure exerted on the solid boundary by the liquid jet can be calculated using the water hammer equation [14]:

$$p_j = \rho_l C_l V_m \left(\frac{\rho_s C_s}{\rho_s C_s + \rho_l C_l}\right) \tag{2}$$

where each ρ is a density, each C is a compression wave velocity, and subscripts s and l refer to solid and liquid, respectively. Usually $\rho_s C_s$, is large compared to $P_l C_l$, the approximation can be deduced from Eq. (2).

$$p_j = \rho_l C_l V_m \tag{3}$$

$$C_s = \sqrt{\frac{E_s}{\rho_s}} \frac{1-\mu}{(1+\mu)(1-2\mu)} \tag{4}$$

And

$$C_l = \frac{1}{\sqrt{\rho_l\left(\frac{1}{E_l} + \frac{D}{eE_s}\right)}} \tag{5}$$

where μ is the Poisson's ratio, E_s the Young's modulus, E_l the bulk elastic modulus of the liquid, and D and e are the inner diameter and thickness, respectively, of the elastic conduit through which the fluid flows.

2.2. Loading spectrum and simulation model

It is very difficult to count the number of collapse

cavitation bubbles and to acquire the accurate loading spectrum near the rigid boundary by the actual engineered hydraulic equipment. Nevertheless, many people have gotten the impact pressure from a single cavitation bubble by means of laser or spark-discharged electrode methods under water [15-16]. Here, the collapsing pressure is recorded by the latter method and the spectrum values are standardized, as shown in Fig. 2.

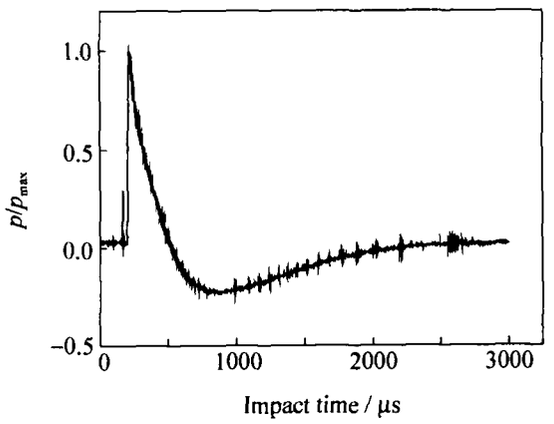

Fig. 2. Loading spectrum generated from the spark-generated bubble collapse near a wall.

Generally, the collapse effects of cavitation bubbles can be divided into two aspects [17]. In the first aspect, high-speed jets strike on the boundary randomly and respectively like dropping water that impacts on the ground, causing material erosion in the form of initial micro pits on the surface. In the second aspect, the impinging jet pressure acts on the groove surfaces or cracks internally and contributes to crack propagation. The sizes of these pits continue to increase and become critical under repeated jet attacks, and micro cracks will emanate from the boundary of the pits.

To fulfill the requirements of numerical simulation, two assumptions were made. First, assuming the pressure P_j is uniformly and vertically distributed on the groove surfaces, and the loading spectrum recorded from the spark-generated bubble is applied to the uniform surfaces. The pressure of numerical loading is 200 MPa. The cross section of the model containing grooves on the surface was created. The model is a rectangular three-dimensional solid, which is 15 mm long, 10 mm high, and 5 mm thick. The rectangular or triangular groove embeds in the middle of the top surface; the rectangular one is shown schematically in Fig. 3. The various cavities or grooves are determined through the change in depth and length.

3. Fatigue theory analysis

The numerical simulation fatigue analysis is based on the proposal by Morrow [18], the relation of the total strain amplitude (ε_a) and the fatigue life in reversals to failure ($2N_f$) can be expressed in the following form:

$$\varepsilon_a = \varepsilon_a^e + \varepsilon_a^p = \frac{\sigma_f'}{E}(2N_f)^b + \varepsilon_f'(2N_f)^c \tag{6}$$

where ε_a^e is the elastic strain amplitude, ε_a^p the plastic strain amplitude, σ_f' the fatigue strength coefficient; b the fatigue strength exponent, usually varying between –0.04 and –0.15 for metals; ε_f' the fatigue ductility coefficient; c the fatigue ductility exponent, usually varying between –0.3 and –1.0 for metals; $2N_f$ the transition fatigue life in reversals.

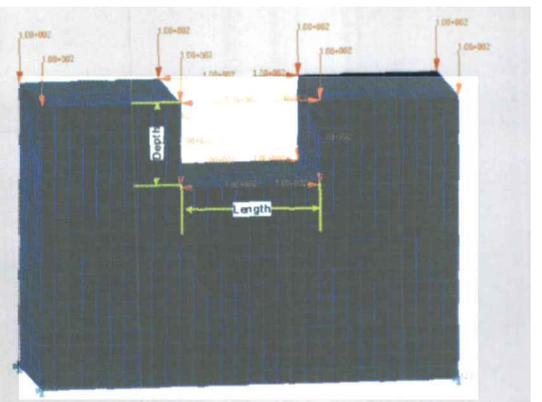

Fig. 3. Loading conditions of cavitation bubble collapse applied to the simple model.

Eq. (6), the strain-lie equation, is the foundation for the strain-based approach for fatigue. This equation is the summation of two separate curves for elastic strain amplitude-life ($\varepsilon_a^e - 2N_f$) and for plastic strain amplitude-life ($\varepsilon_a^p - 2N_f$). Dividing the Basquin equation [19] by the elastic modulus gives the equation for the elastic strain amplitude-life curve:

$$\varepsilon_a^e = \frac{\Delta\varepsilon^e}{2} = \frac{\sigma_a}{E} = \frac{\sigma_f'}{E}(2N_f)^b \tag{7}$$

Both Manson [20] and Coffin [21] simultaneously proposed the equation for the plastic strain amplitude-life curve:

$$\varepsilon_a^p = \frac{\Delta\varepsilon^p}{2} = \varepsilon_f'(2N_f)^b \tag{8}$$

Smith, Watson, and Topper have proposed a slightly different approach to account for the mean stress through a consideration of the maximum stress present in any given cycle [23]. In this case, the damage parameter is taken to be the product of the maximum stress, σ_{max} (here equal to the true stress σ_a, MPa), and the strain amplitude, ε_a, of a cycle.

For fully reversed loading, the maximum stress σ_{max} is given by

$$\sigma_{max} = \sigma_f'(2N_f)^b \tag{9}$$

And by multiplying the strain-life Eq. (6) by this term, we obtain

$$\sigma_{max}\varepsilon_a = \frac{\sigma_f'}{E}(2N_f)^{2b} + \sigma_f'\varepsilon_f'(2N_f)^{b+c} \quad (10)$$

The Smith-Watson-Topper (SWT) equation predicts that no fatigue damage can accrue when the maximum stress becomes zero or negative, which is not strictly true. In this article, the SWT equation method is used to simulate the initiation crack life.

The 304SS and BS4360-50D stainless steels were selected to numerical simulation; the densities of both materials were neglected. Some of the properties of both materials are listed in Table 1.

Table 1. Mechanical properties of the 304SS and BS4360-50D stainless steels

Properties	304SS	BS4360-50D
Yeld stress, YS / MPa	235	355
Ultimate tensile stress, UTS / MPa	100	480
Young's modulus, E_s / MPa	1.86×10^5	1.914×10^5
Elastic Poisson's ratio	0.29	0.30
Fatigue strength exponent, b	–0.15	–0.123
Fatigue ductility exponent, c	–0.77	–0.618
Fatigue strength coefficient, σ_f'	2413	1036

Note: The data from the Ph.D Thesis of Zhu, University of sheffield and British Steel Corporation, UK, 1989.

4. Results and discussion

From the results as illustrated in Fig. 4, the number of cycles decreases rapidly with the extension of crack depth for both materials. When the depth is 4 mm, the fatigue cycle life decreases by 2-3 orders of magnitude than that when the depth is 1 mm. Furthermore, the graph also shows a good relation between the logarithm of cycle life and the depth of the rectangular groove. The 304SS exhibits a higher fatigue resistance than BS4360-50D in the same loading conditions. Similarly, for the triangular groove, the same trend of fatigue life is gained, nevertheless, the fatigue life curves show more jags than those of the rectangular one, which indicates that the cycles of initiation crack life is also determined by other factors besides depth. As predicted, of the two materials the variation in initiation crack life is very distinct for the large difference of fatigue properties.

The true stress amplitude σ_a calculated with Eq. (9) instead of the engineering stress determines the actual loadings on the components, as shown in Fig. 5. It is observed that the BS4360 stainless steel needs much less cycles and lower true stress amplitudes to produce the initiation crack than 304SS. The values of true stress amplitude are increasing with the large groove depth. It implies that those zones are much easily damaged, in other words, the material inhere is speedily detached and eroded. Furthermore, several articles verified it, in which the data of the mass loss rate of materials mostly increased with cavitation erosion time after the incubation period [4, 23].

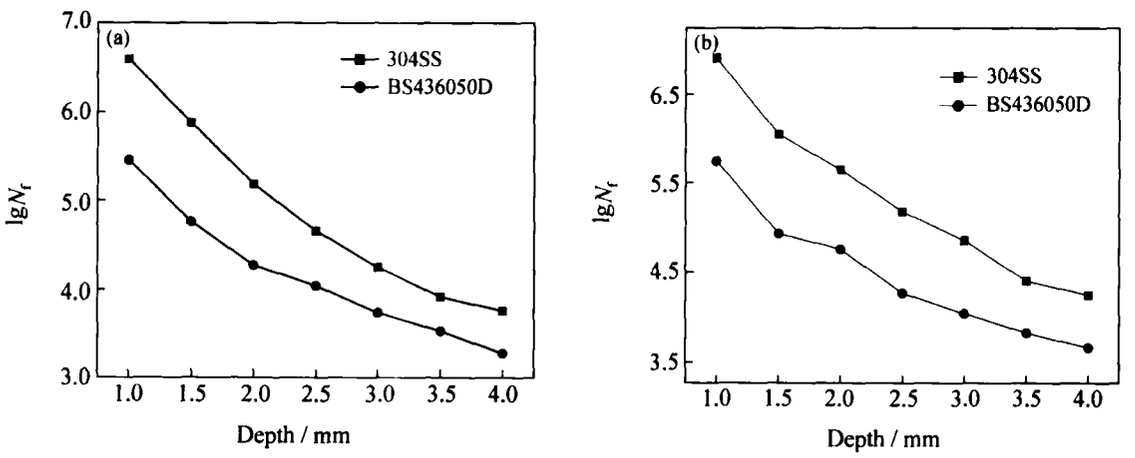

Fig. 4. Cycles of the crack initiation life as a function of the groove depth: (a) rectangular groove; (b) triangular groove.

However, it is not necessarily following the damage rule that the crack length varies while the depth is fixed, as shown in Fig. 6. The possible reason is that the interaction of loadings is on the tip of the triangular groove, which leads to the fluctuant of true stress. From the fatigue cycle life graph, as shown in Fig. 7, the most seriously damaged zones of the rectangular crack groove locate on the two inner sides of the corners; while, for the triangular groove, such a zone always occurs below the bottom tip.

It should be noted that once the cavitation cavity is formed, just as to the simulation graph, the damaged zones always occur at the tip of the pits or corner, which explains the law of crack propagation and the development of peculiar cavitation damage appearance, which looks like a needle hole or inverse sharp cone-shape.

Fig. 8 shows a typical photograph of localized cavitation damage on the surface. It usually has the jagged appearance consistent with the fatigue failure results; this is fairly easy to distinguish from the erosion due to solid particles, which has a much smoother appearance.

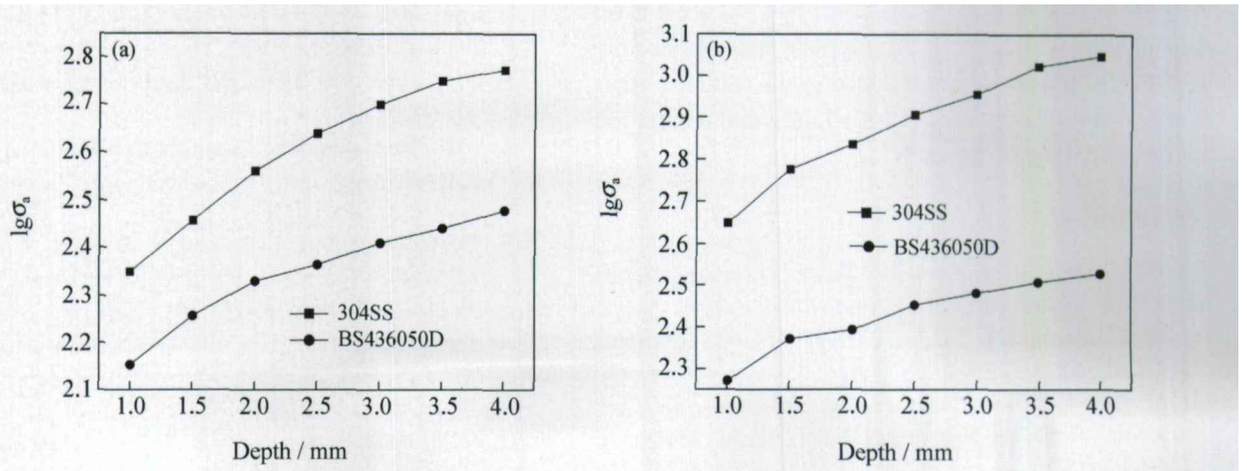

Fig. 5. True stress of the crack initiation life as a function of the groove depth: (a) rectangular groove; (b) triangular groove.

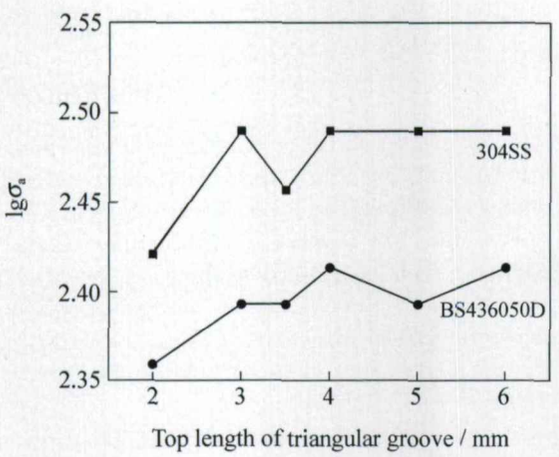

Fig. 6. True stress crack initiation analysis as a function of the triangular groove length.

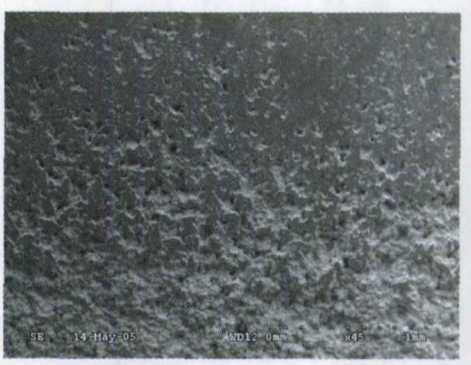

Fig. 7. SEM image of the cavation coatings deposited by AC-HVAF.

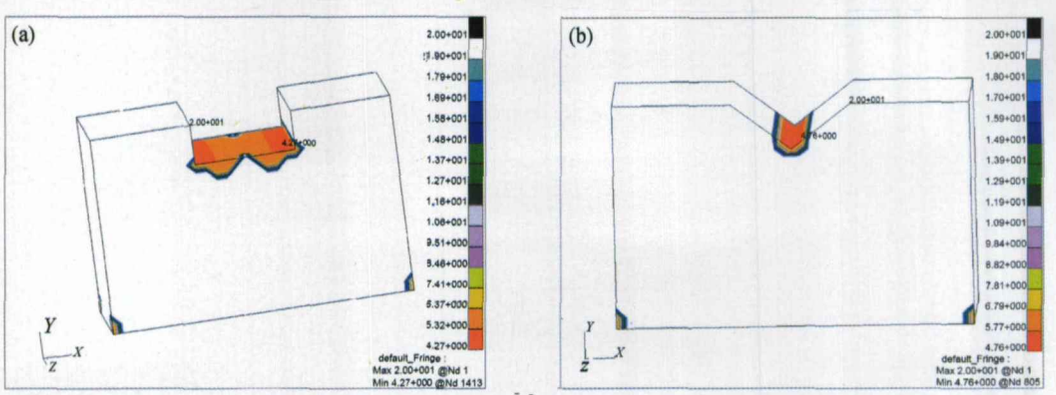

Fig. 8. Distribution of the fatigue life graph along the cycles: (a) rectangular groove; (b) triangular groove.

5. Conclusions

The numerical results demonstrate that the fatigue effects induced by the collapsing bubbles play a significantly role in materials destruction during the cavitation erosion process. Both the bubble collapsing impact damage and the fatigue process will contribute to the accelerating failure of metal materials.

The values of initiation crack life and true stress amplitude are fluctuant with the size of loading area and the angle of tips, and most cavitation fatigue damage spots are located below the tip of triangular, which provides a new explanation to the characteristic damaged appearance of cavitation pits. Furthermore, fatigue effect leads the crack to propagate progressively with a certain direction, which has been verified

by many experiments.

Although the present fatigue model is predictive, the direct detachment effect of microjet impact and the thermal concentration in cavitation bubbles are not yet considered, and several assumptions are not exactly accurate to the cavitation models. In the future, further work needs to complete the fully numerical simulation model of cavitation erosion.

References

[1] C.E. Brennen, *Cavitation and Bubble Dynamics*, Oxford University Press, New York, 1995.

[2] A. Karimi and J.L. Martin, Cavitation erosion of metals, *Int. Met., Rev.*, 31(1986), No.1, p.1.

[3] W. Liu, Y.G. Zheng, and C.S. Liu, Cavitation erosion behavior of Cr-Mn-N stainless steels, *Wear*, 254(2003), No.7-8, p.713.

[4] R.T. Knapp, J.W. Daily, and F.G. Hammitt, *Cavitation*, McGraw-Hill Inc., New York, 1970.

[5] Z.Y. Wang and J.H. Zhu, Cavitation erosion of Fe-Mn-Si-Cr shape memory alloys, *Wear*, 256(2004), No. 1-2, p.66.

[6] Y. Zhang, Z.C. Wang, and Y. Cui, The cavitation behavior of a metastable Cr-Mn-Ni Steel, *Wear*, 240(2000), No.1-2, p.231.

[7] R.H. Richman and W.P. McNaughton, Correlation of cavitation erosion behavior with mechanical, *Wear*, 140(1990), No.1, p.63.

[8] L. Rayleigh, On the pressure developed in a liquid during the collapse of a spherical cavity, *Phil. Mag.*, 34(1917), p.94.

[9] T.B. Benjamin and A. Ellis, The collapse of cavitation bubbles and the pressures thereby produced against solid boundaries, *Philos. Trans. R. Soc. Lond.*, A260(1966). No.1110, p.221.

[10] J.R. Blake, B.B. Taib, and G. Doherty, Transient cavities near boundaries: Part 1. Rigid boundary, *J. Fluid. Mech.*, 170(1988), p.479.

[11] J.R. Blake and D.C. Gibson, Cavitation bubbles near boundaries, *Ann. Rev. Fluid Mech.*, 19(1987), p.99.

[12] J.R. Blake, P. Cerone, A note on the impulse due to a vapor bubble near a boundary, *J. Aust. Math. Soc. B*, 23(1982), p.383.

[13] A. Pearson, J.R. Blake, and S.R.Otto, Jet in bubbles, *J. Eng. Math.*, 48(2004), p.391.

[14] M.S. Plesset and R.B. Chapman, Collapse of an initially spherical vapour cavity in neighborhood of a solid boundary, *J. Fluid Mech.*, 47(1971), p.283.

[15] T. Momma and A. Lichtarowicz, A Study of pressures and erosion produced by collapse cavitation, *Wear*, 186-187(1995), No.2, p.425.

[16] A. Shima, K. Takayama, and Y. Tomita, Mechanism of impact pressure generation from spark-generated bubble collapse near a wall, *AIAA J*, 21(1983), No.1, p.55.

[17] F. Wu , H.C. Hwang, and Y.K. Lin, A fracture mechanics model for cavitation damage in mechanical heart valve prostheses, *Cardiov. Eng.*, 1(2001), No.4, p.171.

[18] J.D. Morrow, Cyclic plastic strain energy and fatigue of metals, [in] *Internal Friction, Damping, and Cyclic Plasticity*, ASTM-STP, PA, 1965, p.45

[19] H. Basquin, The exponential law of endurance tests, *Proc. ASTM*, 10(1910), p.625.

[20] S.S. Manson, Behaviour of materials under conditions of thermal stress, [in] *Heat Transfer Symposium*, University of Michigan Engineering Research Institute, 1953, p.9.

[21] L.F. Coffin, The problem of thermal stress fatigue in austenitic steels at elevated temperatures, *ASTM STP*, 165(1954), p.31.

[22] K.N. Smith, P. Watson, and T.H. Topper, A stress-strain function for the fatigue of metals, *J. Mater.*, 5(1970), No.4, p.767.

[23] S.C. Chang, W.H. Weng, and H.C. Chen, The cavitation erosion of Fe-Mn-Al alloys, *Wear*, 181-183(1995), No.2, p.511.